A random model of anisotropic hydraulic conductivity tailored to the InSAR-based analysis of aquifers

Sona Salehian Ghamsari[1*], Tonie van Dam[2] and Jack S. Hale[1]

[1]Department of Engineering, Faculty of Science, Technology, and Medicine, University of Luxembourg, 6 avenue de la Fonte, Esch-sur-Alzette, L-4364, Luxembourg.

[2]Department of Geology and Geophysics, College of Mines and Earth Sciences, University of Utah, 201 Presidents' Circle, Salt Lake City, 84112-0102, Utah, United States.

Abstract

Sustainable aquifer management depends on reliable predictive models calibrated against diverse sources of data. Poroelastic coupling between fluid flow and surface displacement in an aquifer indicates that precise Interferometric Synthetic Aperture Radar (InSAR) displacement observation can be used to calibrate lateral hydraulic conductivity values. While previous Bayesian inference approaches to this problem have assumed isotropic random models for the hydraulic conductivity, many aquifers are characterized by strong anisotropic hydraulic conductivity (AHC). Consequently, isotropic models are in many cases inadequate. Leveraging a recently proposed Lie group approach for constructing random symmetric positive definite matrices, we propose a new random model for describing AHC in aquifer systems that can incorporate directional information from complex and potentially multi-modal structural geological data. We apply this methodology to describing two conceptual states of uncertainty at the 1996 Anderson Junction aquifer pump test where both multi-modal circular fracture outcrop and AHC principal magnitude data is available. After calibration against this data, the induced uncertainty in AHC is propagated through a partial differential equation-based conceptual model of the test. Our results show that the proposed methodology provides a flexible tool for modeling the effect of uncertain anisotropic hydraulic conductivity on InSAR-measurable surface displacements. Complete open source scripts using the DOLFINx finite element solver and numpyro/JAX are given as supplementary material.

Keywords: predictive hydrological modeling, uncertainty, Interferometric Synthetic Aperture Radar (InSAR), symmetric positive definite tensors.

1 Introduction

Water extracted from aquifers is essential for drinking water, agriculture and industry (Food and Agriculture Organization of the United Nations (FAO) 2022). However over-exploitation presents a major threat to sustainability (Basu and Van Meter 2014; Caretta et al. 2022), with adverse consequences including land subsidence (Heilweil and Hsieh 2006; Burbey et al. 2006; Galloway and Burbey 2011), reduced water availability (Walker et al. 2020) and salt water intrusion (Guo et al. 2019). Therefore, water management, supported by predictive computational models calibrated against all available data sources, is an important part of ensuring the future sustainability of the Earth's water resources (Singh 2014; Amitrano et al. 2014).

In recent years, the remote sensing methodology Interferometric Synthetic Aperture Radar (InSAR) has become popular for acquiring data about ground surface displacements due to its wide spatial coverage, cost-effectiveness and non-invasive nature (Massonnet and Feigl 1998; Tomás et al. 2014). Because the coupling between the solid skeleton of the sedimentary rocks and the fluid flowing through the aquifer's pores, it has been proposed (Burbey et al. 2006; Burbey 2006; Alghamdi 2020) that geodetic surface displacement data derived from methodologies such as InSAR and Global Positioning System (GPS) may contain valuable information for inferring the lateral hydraulic conductivity field of an aquifer.

Focusing on work exploring inverse problems and surface displacment data for inferring aquifer hydraulic conductivity, a series of recent papers (Hesse and Stadler 2014; Alghamdi et al. 2020, 2021, 2024) introduced a scalable Bayesian inversion framework that uses a log–Gaussian process prior model (Tarantola 2005; Fernández-Martínez et al. 2013) to infer from a heterogeneous *isotropic* hydraulic conductivity field from InSAR displacement data. However, in many aquifers the hydraulic conductivity exhibits anisotropy due to networks of lower scale flow-promoting features such as cracks and faults (Hurlow 1998; Berre et al. 2019). In the subjective Bayesian approach to inverse problems (Tarantola 2005) the choice of prior is critical in drawing conclusions from the posterior, after incorporating data via the likelihood. Consequently, the isotropic prior model imposed on the hydraulic conductivity field in Alghamdi et al. (2020, 2021, 2024) may be a unsuitable when field studies indicate that flow at the site is likely anisotropic (Pollard and Fletcher 2005).

In Salehian Ghamsari et al. (2025) we investigated the link between aquifer anisotropic hydraulic conductivity (AHC) and InSAR derived surface displacements by constructing a poroelastic partial differential equation (PDE)-based model of the Anderson Junction aquifer test, which was determined be strongly anisotropic during a pump test described in Heilweil and Hsieh (2006). We used forward modelling to determine that site-scale AHC would lead to distinctive elliptical displacement patterns at the surface that, with correct pump test conditions, could be detected using InSAR. Consequently, our hypothesis is that InSAR data contains valuable information for

inferring AHC and that it is necessary to develop random models of AHC tailored for InSAR-based aquifer analysis. To address this gap, in this paper we develop a random model on the AHC tensor that could be used as a prior in a subjective Bayesian inference setting to assimilate InSAR data. In the following paragraphs, we outline the key points of and justification for our development using the Anderson Junction pumping test described in Heilweil and Hsieh (2006) as a foundational element.

In the original study (Heilweil and Hsieh 2006) describing the Anderson Junction aquifer pumping test, the authors proposed a modified Papadopulus method (Papadopulos 1965) to infer the magnitude of the hydraulic conductivity in the direction of two pressure observation wells *assumed* to be aligned with the principal directions of AHC[1]. Heilweil and Hsieh (2006) used the predominant fracture azimuths determined from a circular histogram which we reproduce (rose diagram in Fig. 1) to decide where the observation wells should be drilled. The fracture data reveals two nearly-orthogonal primary modes – consequently well A was drilled approximately along the direction of the first primary mode (x direction). Well B was drilled orthogonal to the x direction (y direction), a constraint imposed by the modified Papadopulus method rather than being driven by statistics of the rose diagram (more on this below). After observing the pressure drop data and calculating the two principal hydraulic conductivities, the major and minor directions were assigned to the x and y directions, respectively.

There are limitations to the analysis of the fracture data in Heilweil and Hsieh (2006). Firstly, as noted by Heilweil and Hsieh (2006), the principal direction is inherently uncertain and so if well A is not in fact aligned with the principal direction, then this directional uncertainty will introduce further uncertainty in the inferred principal values of the anisotropic hydraulic conductivity. This fact supports the motivation for developing a random model that can represent uncertainty in the principal direction. Secondly, although Heilweil and Hsieh (2006) indicate that it is 'neither necessary (nor warranted) to assume which is the major and which is the minor principal direction at the start of the analysis', it is not always the case that there are two or more nearly orthogonal fracture sets that allows well B to be simultaneously aligned with the secondary primary fracture mode *and* be orthogonal to well A. This observation supports the development of a random model that can represent multi-modal and/or non-orthogonal fracture sets. Finally, we note that when using InSAR to infer AHC for any prior model to be useful it should not be necessary to assume which direction is the major and minor one *a priori*. As we will show here, the proposed random model of AHC can naturally support these diverse states of uncertainty.

The fracture data discussed in the previous paragraphs represent a circular random variable. Circular random variables are increasingly used in the earth sciences to represent directional data (Adler and Thovert 1999; Lark et al. 2014; Rad et al. 2022). Circular random variables are distributed on the unit circle, characterized by the property that the upper limit is topologically close to the lower limit. This distinctive feature necessitates specialized approaches for all aspects of statistical analysis,

[1]In the original Papadopulos (1965) method no assumption is made on the alignment of the wells with respect to the principal directions of AHC thus a minimum of three, rather than two, observation wells are required to uniquely determine the AHC tensor.

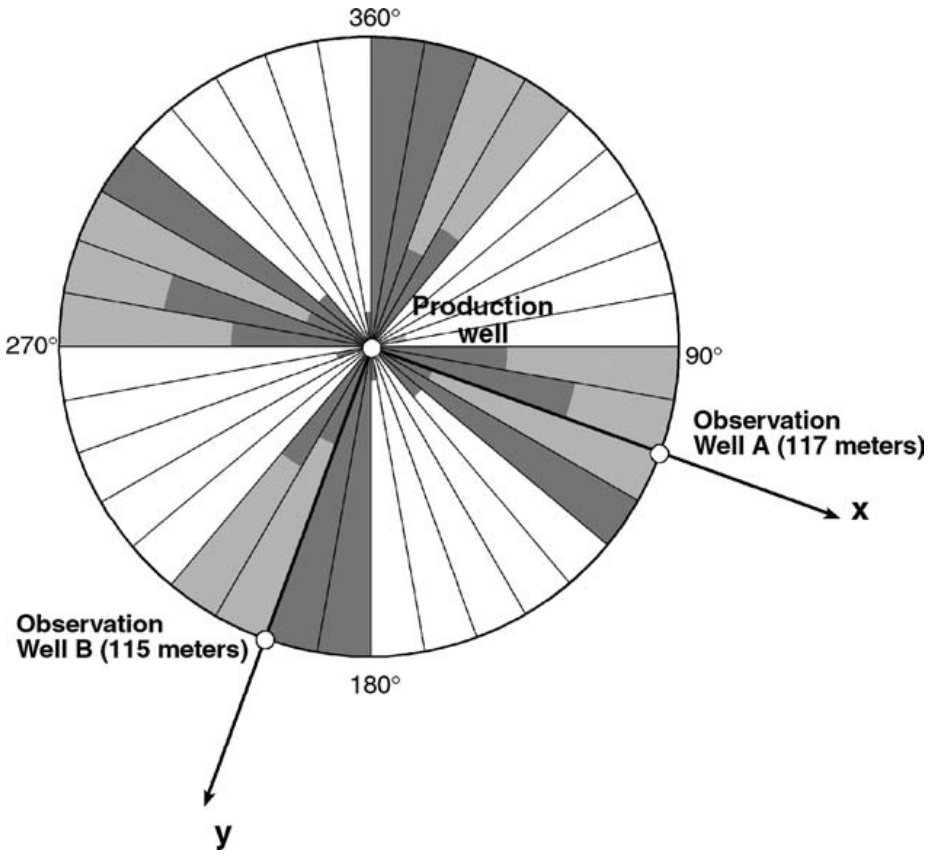

Fig. 1: Rose diagram (circular histogram) summarising fracture orientations and locations of the observation wells at Anderson Junction. We remark on the two primary modes along the x and y axis, and the two submodes along the x axis. Figure reproduced from Heilweil and Hsieh (2006).

see e.g. Mardia and Jupp (1999); Ley and Verdebout (2017) for a full treatment. Examples of circular random variables include gene expression (Taghia et al. 2014) and wind direction data (Rad et al. 2022). Returning to structural geological data (Pollard and Fletcher 2005), Lark et al. (2014) were the first to propose using a mixture of von Mises distributions (Pewsey and García-Portugués 2021) within a frequentist maximum likelihood estimation (MLE) framework to capture complex multimodal directional data, and thereby extending the earlier unimodal construction of Davis (2002).

The first contribution of this paper is to develop a Bayesian model for potentially multi-modal directional structured geological data. This model will be calibrated

against the fracture data acquired at the Anderson Junction site (Heilweil and Hsieh 2006) to produce a random model of the principal direction of the AHC tensor. The proposed model consists of a collection of circular von Mises distributions with unknown means and variances that are then mixed with weights modeled using a Dirichlet distribution (Bishop 2006, Chapter 9). In contrast to the non-probabilistic analysis of the fracture outcrop data performed in the original study of Heilweil and Hsieh (2006), our model is capable of capturing uncertainty in the principal direction and the multi-modality present in the original data. Additionally, it is able to represent fracture sets (modes) that are non-orthogonal. Aside from some structural differences that we discuss later, a distinct methodological difference between our work and Taghia et al. (2014) is that we use a Markov chain for posterior exploration, rather than variational inference (VI) (Blei et al. 2017). Further, we include an alternative approach for determining model complexity (here, the strict number of mixtures) based on Leave-one-out cross-validation (LOOCV) (Mao et al. 2014), rather than reversible jump MCMC (Mulder et al. 2020) or ELBO (Taghia et al. 2014).

The poroelastic model of the Anderson Junction pump test described in Salehian Ghamsari et al. (2025) is parameterised by the AHC tensor. For this model to be well-posed, the AHC tensor must be symmetric positive definite (SPD). To convert the stochastic model of the principal direction to an SPD tensor we follow an approach for constructing random SPD second-rank tensors as proposed in (Shivanand et al. 2024). In short, the SPD AHC tensor undergoes spectral decomposition – its positive eigenvalues represent the strength of the hydraulic conductivity along the principal axis, while its orthogonal eigenvectors capture its orientation. The eigenvectors are parameterized by a (random) angle, the eigenvalues by (random) strictly positive reals, and the SPD property of the random AHC tensor is then guaranteed by a rigorous Lie group derivation. Importantly for our application, this construction allows for separate control of magnitude and direction, facilitating the representation of complex anisotropy like that induced by the directional model described in the previous paragraph.

To demonstrate the flexibility of our development, we construct two conceptual states of uncertain AHC based on data from the Anderson Junction site. In the first setting, we assume knowledge of the fracture outcrop data and the magnitude of AHC in the principal directions inferred in Heilweil and Hsieh (2006) – this allows us to only consider the first primary mode in the x-direction. In the second setting, we assume that we do not posses knowledge of the magnitudes of AHC, so the major direction could be in either the x or y-direction. For the two cases, we calculate summary statistics of the InSAR Line of Sight (LOS) surface displacement to evaluate the influence of AHC uncertainty. The results indicate that the uncertainty is greatest in regions far from the pumping well and that directional uncertainty leads to potentially complex standard deviation patterns in space and time, underscoring the importance of modelling uncertain AHC on the subsidence response of an aquifer.

In summary, the main contributions of our paper are as follows:

1. We introduce a Bayesian mixture model for the rotation angle representing the complex multi-directional fracture data at Anderson Junction. This extends the

frequentist approach for fitting structural geology data originally described in Lark et al. (2014) to a Bayesian setting.
2. Leveraging the Bayesian rotation angle model we extend the Lie group construction of SPD tensors proposed in Shivanand et al. (2024) to more complex anisotropic settings, including multi-modal principal directions.
3. We show that our AHC model is sufficiently flexible to replicate two conceptual states of knowledge about the Anderson Junction site.
4. We propagate the resulting uncertainty through a poroelastic model of the pump test and show that uncertain AHC leads to a substantial impact on the model's prediction of InSAR LOS displacements.

Although our method is applied to a hydrological problem, the overall approach is relatively general and could be applied to other settings where complex uncertainty in an anisotropic second-rank tensor quantity is present (Guilleminot and Soize 2012; Guilleminot et al. 2012; Shivanand et al. 2024).

This paper is structured as follows: Section 2 provides an overview of the Anderson Junction study area, focusing on the aquifer pumping test and fracturing observed in this area. In section 3, we detail the methodology, including the PDE-based forward model, the parametric Bayesian model for fracture outcrop data, the construction of a model for the AHC tensor, and finally the forward uncertainty analysis through the PDE-based forward model. The implementation and results are presented in section 4, before we conclude in section 5.

2 Case study

In this section, we restate the main features of the Anderson Junction aquifer pumping test, Utah, USA, see fig. 2 (Hurlow 1998; Heilweil and Hsieh 2006; Salehian Ghamsari et al. 2025). The test used a pumping well and two observation wells, assumed to be aligned with the principal directions of AHC, to estimate the major and minor hydraulic conductivity of the confined Navajo sandstone aquifer. Groundwater extraction from the pumping well occurred over a period of four days at an average rate of $0.07\,\mathrm{m}^3\,\mathrm{s}^{-1}$. Salehian Ghamsari et al. (2025) predicted that the vertical surface displacement induced by this pumping would likely be insufficient to be detected using Sentinel-1 InSAR. To address this limitation, we designed a hypothetical scenario where pumping occurred at $0.28\,\mathrm{m}^3\,\mathrm{s}^{-1}$ for 8 days – this rate is used in our numerical experiments in this paper.

Figure 1 summarizes the relative frequency of fracture directions (azimuths) in the Navajo Sandstone. The first fracture mode (x direction) is oriented towards the north at 180° to 210° and the second fracture mode (y direction) at 90° to 130°. After acquiring pressure drop data at the observation wells, Heilweil and Hsieh (2006) estimated the hydraulic conductivity in the major principal direction as $k_{xx} = 1.1 \times 10^{-8} \pm 21\%\ \mathrm{m}^3\,\mathrm{s}\,\mathrm{kg}^{-1}$ and in the minor direction $k_{yy} = 4.7 \times 10^{-10} \pm 19\%\ \mathrm{m}^3\,\mathrm{s}\,\mathrm{kg}^{-1}$. Hydraulic conductivity is an intrinsic property of the aquifer, independent of pumping rate. Thus, we use these inferred conductivities in our hypothetical scenario.

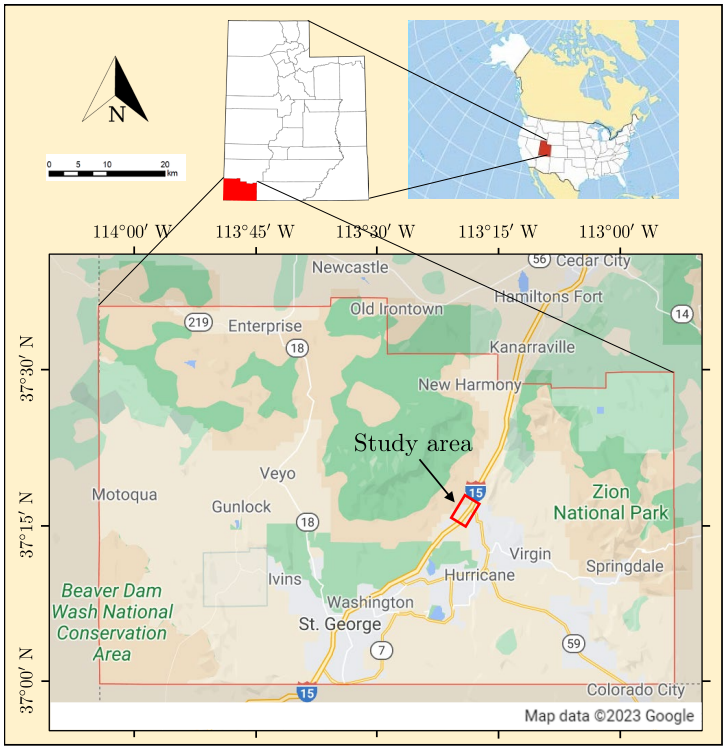

Fig. 2: Location of the Anderson Junction aquifer in Utah, USA. Used under CC BY 4.0 license from Salehian Ghamsari et al. (2025). Map data ©2023 Google.

3 Methodology

In fig. 3, we outline the key elements of our proposed methodology. In this section, we discuss the mathematical aspects of the model. The calibration and application to the Anderson Junction site is left for section 4.

3.1 Poroelastic finite element model

We first outline the three-field finite element formulation (Brenner and Scott 2008) of Biot's poroelasticity theory following Ferronato et al. (2010) and Alghamdi (2020). The PDE system is discretized using finite elements and the solver implemented in the DOLFINx finite element problem solving environment (Baratta et al. 2023; Scroggs et al. 2022,?; Alnaes et al. 2014; Kirby and Logg 2006). Further technical details are given in (Salehian Ghamsari et al. 2025, Appendix A) and (Salehian Ghamsari and Hale 2024b).

Given a domain $\Omega \subset \mathbb{R}^3$ with boundary Γ and outward-pointing normal n find the fluid-pore pressure $p : \Omega \times (0, T] \to \mathbb{R}$, deformation $u : \Omega \times (0, T] \to \mathbb{R}^3$ and fluid flux

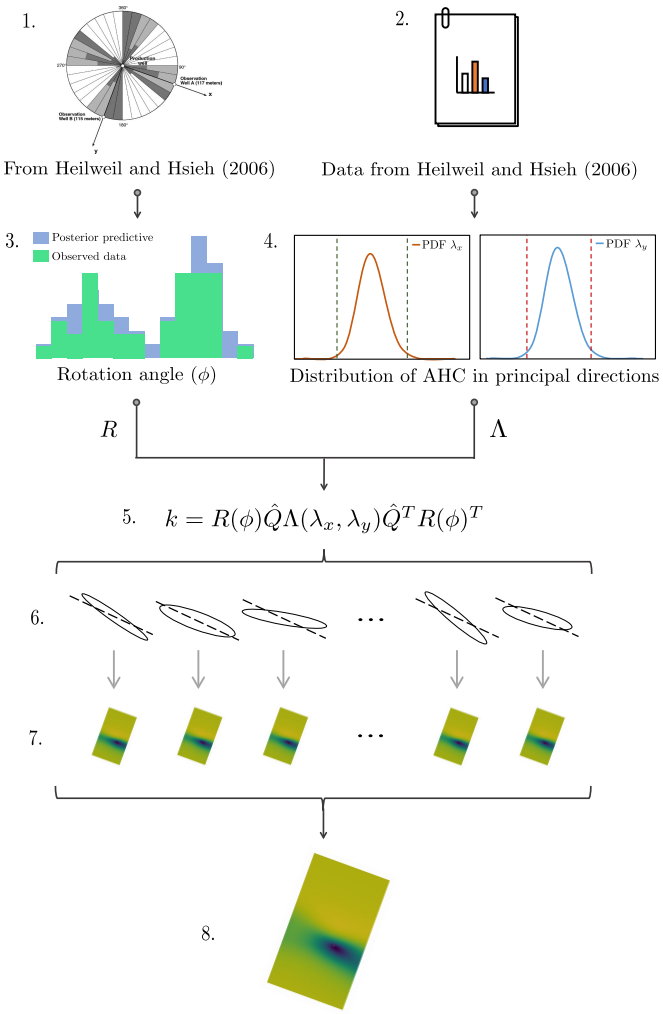

Fig. 3: Overview of methodology. 1. Principal direction data from structural geological data; 2. Data on hydraulic conductivity in principal directions; 3. Calibration of Bayesian model for rotation angle from structural geological data; 4. Calibration of model on hydraulic conductivity in principal directions using hydraulic conductivity data; 5. and 6. Using calibrated models from 3. and 4. generate random SPD AHC tensors; 7. Propagate uncertainty induced by AHC tensor through the conceptual model of Anderson Junction aquifer system; 8. Summary statistics of the InSAR LOS displacement.

$q : \Omega \times (0, T] \to \mathbb{R}^3$ such that

$$(S_\epsilon p + \alpha \nabla \cdot u)_t + \nabla \cdot q = f_p \text{ on } \Omega \times (0, T], \tag{1a}$$
$$-\nabla \cdot \bar{\sigma}(u, p) = f_u \text{ on } \Omega \times (0, T], \tag{1b}$$
$$q + \widetilde{k} \nabla p = 0 \text{ on } \Omega \times (0, T], \tag{1c}$$

with boundary conditions on disjoint parts of the boundary for both the solid problem $\Gamma = \Gamma_u^d \cup \Gamma_u^n$ and the fluid problem $\Gamma = \Gamma_p^d \cup \Gamma_p^n$ given by

$$\begin{aligned} u &= u_d \text{ on } \Gamma_u^d \times (0, T], \\ \bar{\sigma} \cdot n &= g_u \text{ on } \Gamma_u^n \times (0, T], \\ p &= p_d \text{ on } \Gamma_p^d \times (0, T], \\ q \cdot n &= g_p \text{ on } \Gamma_p^n \times (0, T], \end{aligned}$$

and initial conditions

$$\begin{aligned} p(x, 0) &= p^0 \text{ on } \Omega, \\ u(x, 0) &= u^0 \text{ on } \Omega, \\ q(x, 0) &= q^0 \text{ on } \Omega. \end{aligned}$$

The small strain and stress tensors for isotropic linear elasticity are given by

$$\varepsilon = \frac{1}{2} \left(\nabla u + (\nabla u)^T \right), \tag{2a}$$
$$\sigma = 2\mu_s \varepsilon + \lambda (\operatorname{Tr} \varepsilon) I, \tag{2b}$$

respectively, and the Biot stress tensor as

$$\bar{\sigma} = \sigma - \alpha p I, \tag{3}$$

All further notations, parameters and units are given in table 1. The actual domain, boundaries, initial conditions and parameter values for the site are provided in section 4.1.

To represent the AHC tensor $\tilde{k}$ in eq. (1) using vector and matrix notation, we specify the three-dimensional Euclidean space with mutually orthogonal axes (x, y, z). The x-axis and y-axis are aligned with the directions x and y shown in fig. 1. The z-axis points downward into the earth. Unless otherwise stated, all first- and second-ranked tensor-valued quantities in the paper are written as vectors and matrices, respectively, with respect to this Euclidean space.

We calculate the displacement in the LOS direction of Synthetic Aperture Radar (SAR) data. This technique uses radar pulses emitted in the LOS direction, perpendicular to the satellite's motion. Following Fuhrmann and Garthwaite (2019), we use

Symbol	Description	Units
$()_t$	time derivative	s^{-1}
∇	gradient operator	m^{-1}
$\nabla\cdot$	divergence operator	m^{-1}
Tr	trace operator	dimensionless
$(\cdot)^T$	transpose operator	dimensionless
p	fluid pore pressure	Pa
u	elastic deformation	m
q	volumetric fluid flux	$\mathrm{m\,s}^{-1}$
f_p	fluid source density	s^{-1}
g_p	boundary fluid flux	$\mathrm{m\,s}^{-1}$
f_u	body force density	$\mathrm{N\,m}^{-3}$
g_u	traction	Pa
σ	linear elastic stress tensor	Pa
$\bar{\sigma}$	Biot stress tensor	Pa
I	identity tensor	dimensionless
α	Biot coefficient	dimensionless
S_ϵ	drained storage coefficient	Pa^{-1}
$\tilde{k}$	hydraulic conductivity tensor	$\mathrm{m}^3\,\mathrm{s\,kg}^{-1}$
k	2×2 hydraulic conductivity tensor	$\mathrm{m}^3\,\mathrm{s\,kg}^{-1}$
μ_s	drained shear modulus	Pa
λ	second Lamé parameter	Pa

Table 1: Table of main notations and units used in the three-field formulation of Biot's poroelasticity theory. Used under CC BY 4.0 license from Salehian Ghamsari et al. (2025).

the incidence angle θ and satellite heading angle α_h to calculate LOS displacement

$$u_{\mathrm{LOS}} = \begin{bmatrix} -\sin\theta\cos\alpha_h & \sin\theta\sin\alpha_h & \cos\theta \end{bmatrix} \begin{bmatrix} u_E \\ u_N \\ u_U \end{bmatrix}. \tag{4}$$

where u_E, u_N, and u_U represent deformation in the East, North, and Up directions. Surface displacements are derived by transforming the predicted displacements in the model coordinate system to the East-North-Up (ENU) coordinate system.

3.2 The anisotropic hydraulic conductivity (AHC) tensor

We define the space of real-valued symmetric second-rank tensors (matrices) as

$$\mathrm{Sym}(d) := \{k \in \mathbb{R}^{d\times d} \mid k_{ij} = k_{ji}\}, \tag{5}$$

and the subset of positive definite tensors as

$$\mathrm{Sym}^+(d) := \{k \in \mathrm{Sym}(d) \mid z^T k z > 0,\ \forall z \in \mathbb{R}^d \setminus \{0\}\}. \tag{6}$$

To guarantee that eq. (1) is well posed, the AHC tensor $\tilde{k}$ must be a member of $\mathrm{Sym}^+(3)$. We assume that one of the eigenvectors of $\tilde{k}$ is aligned with the z-axis and thus $k_{xz} = k_{yz} = 0$. In this case we have $\tilde{k}$

$$\tilde{k} = \left[\begin{array}{cc|c} k_{xx} & k_{xy} & 0 \\ k_{yx} & k_{yy} & 0 \\ \hline 0 & 0 & k_{zz} \end{array}\right], \tag{7}$$

where the lines in the tensor emphasize the natural block structure. The random modeling in our paper will focuses on the top left block of $\tilde{k}$, which we denote $k \in \mathrm{Sym}^+(2)$, and represents uncertainty in the AHC in the x–y plane. Alghamdi (2020) noted that InSAR displacement data provides little information for inferring k_{zz}. Therefore we treat k_{zz} as perfectly known (non-random).

The arguments presented in Shivanand et al. (2024) lead to a natural parametrization of $k \in \mathrm{Sym}(2)$ in terms of a clockwise rotation angle ϕ in the $x - y$ plane about the z-axis and two positive eigenvalues λ_x and λ_y. We focus here on basic notions that apply in both the deterministic and random setting, and return to the specifics of the stochastic construction in section 3.5. We begin by defining the space of diagonal tensors as

$$\mathrm{Diag}^+(d) := \left\{\Lambda \in \mathbb{R}^{d\times d} \mid \Lambda = \mathrm{diag}(\lambda_1, \lambda_2, \ldots, \lambda_d),\ \lambda_i \in \mathbb{R}^+_*\right\}, \tag{8}$$

where $\mathbb{R}^+_*$ is the space of strictly positive real numbers. The space of orthogonal tensors

$$\mathrm{O}(d) := \left\{Q \in \mathbb{R}^{d\times d} \mid Q^T Q = I\right\}, \tag{9}$$

the subset of special orthogonal tensors

$$\mathrm{SO}(d) := \left\{R \in \mathrm{O}(d) \mid \det(R) = 1\right\}, \tag{10}$$

and its Lie algebra of skew-symmetric tensors

$$\mathfrak{so}(d) := \left\{W \in \mathbb{R}^{d\times d} \mid W^T = -W\right\}. \tag{11}$$

We also define the unit circle

$$\mathbb{S}^1 = \left\{(\cos(\phi), \sin(\phi)) \mid \phi \in [0, 2\pi)\right\}. \tag{12}$$

Any $k \in \mathrm{Sym}^+(2)$ can be decomposed into a tensor $\Lambda := \mathrm{diag}(\lambda_x, \lambda_y) \in \mathrm{Diag}^+(2)$ of eigenvalues and an tensor of eigenvectors $Q \in \mathrm{O}(2)$

$$k = Q\Lambda Q^T. \tag{13}$$

We can further rotate the eigenvectors Q by applying a rotation tensor $R \in \mathrm{SO}(2)$

$$k = (RQ)\Lambda(RQ)^T, \tag{14}$$

It is this decomposition that forms the basis of the stochastic construction in Shivanand et al. (2024). Using the rotation angle ϕ about the z-axis we construct an infinitesimal rotation tensor $W \in \mathfrak{so}(2)$ as

$$W = \phi \begin{bmatrix} 0 & -1 \\ 1 & 0 \end{bmatrix}. \tag{15}$$

Following Hall (2015), it is possible to connect the space $\mathrm{SO}(d)$ with its Lie algebra $\mathfrak{so}(d)$ through the map $\exp : \mathfrak{so}(d) \to \mathrm{SO}(d)$, leading to

$$R = \exp(W). \tag{16}$$

As a consequence of the Cayley-Hamilton theorem (Axler 2024), the Euler-Rodrigues formula gives

$$R = \exp(W) = I + \frac{\sin\phi}{\phi} W + \frac{1 - \cos\phi}{\phi^2} W^2, \tag{17}$$

which reduces to the standard result linking a rotation angle with a rotation matrix

$$R = \begin{bmatrix} \cos\phi & -\sin\phi \\ \sin\phi & \cos\phi \end{bmatrix}. \tag{18}$$

This construction can be extended to the more general three-dimensional case without the block structure in eq. (7). By parametrizing R using two angles ϕ and η, the latter representing a tilt around the y-axis, we can incorporate uncertainty about an additional preferential direction, for example, in a bedding plane dip angle.

3.3 Rotation angle model

In this subsection we develop a hierarchical Bayesian model for the rotation angle ϕ used in eqs. (14) to (16). Throughout the rest of the paper we use a hat $\hat{\cdot}$ to emphasize that a quantity is non-stochastic, i.e. is perfectly known.

To model potentially multi-modal directional data, a mixture of circular von Mises distributions is a suitable choice (Ley and Verdebout 2017; Taghia et al. 2014). We write the joint random model for $n \geq 1$ mixtures on the latent parameters $\theta^n = (\mu_1, \kappa_1, c_1, w_1, m_1 \ldots, \mu_n, \kappa_n, c_n, w_n, m_n)$ and p independent and identically distributed (iid) rotation angles $\phi_1, \phi_2, \ldots, \phi_p$

$$\mu_1, \ldots, \mu_n \overset{\text{iid}}{\sim} \text{VonMises}(\hat{\mu}, \hat{\kappa}), \tag{19a}$$
$$\kappa_1, \ldots, \kappa_n \overset{\text{iid}}{\sim} \text{Gamma}(\hat{\alpha}, \hat{\beta}), \tag{19b}$$
$$c_1, \ldots, c_n \overset{\text{iid}}{\sim} \text{VonMises}(\mu_i, \kappa_i), \tag{19c}$$
$$w_1, \ldots, w_n \sim \text{Dirichlet}(\hat{a}_1, \ldots, \hat{a}_n), \quad n \geq 2, \tag{19d}$$
$$w_1 = 1, \quad n = 1, \tag{19e}$$
$$m_1, \ldots, m_n \sim \text{Categorical}(w_1, \ldots, w_n), \tag{19f}$$
$$\phi_1, \phi_2, ..., \phi_p \overset{\text{iid}}{\sim} \text{Mixture}((m_1, \ldots, m_n), (c_1, \ldots, c_n)), \tag{19g}$$

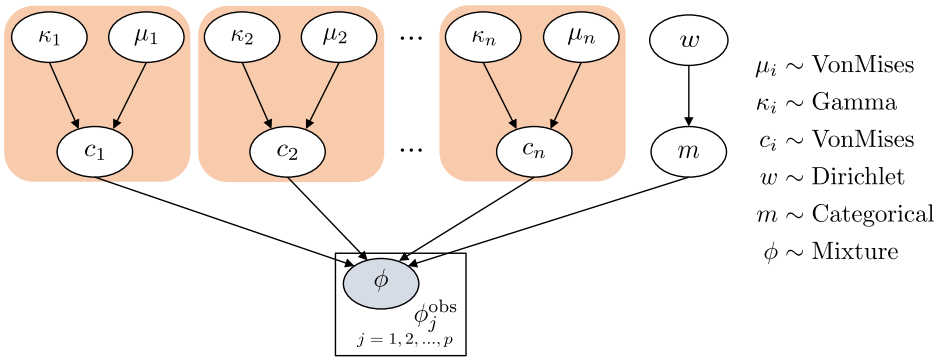

Fig. 4: DAG of the mixture of von Mises model for $n \geq 2$ mixtures. The square boxes denote fixed or observed quantities, and the circles denote unknowns.

which in the case of $n = 1$ (i.e., no mixtures) reduces to

$$\begin{aligned} \mu_1 &\sim \text{VonMises}(\hat{\mu}, \hat{\kappa}), \\ \kappa_1 &\sim \text{Gamma}(\hat{\alpha}, \hat{\beta}), \\ \phi_1, \phi_2, ..., \phi_p &\overset{\text{iid}}{\sim} \text{VonMises}(\mu_1, \kappa_1). \end{aligned}$$

The hierarchical model for the $n \geq 2$ case is visualised as a directed acyclic graph (DAG) in fig. 4. Here, we summarize the components, parameterization and structure of the model. We do not show explicit expressions for the probability density function (PDF) associated with each component, as these are relatively standard, and instead refer the reader to e.g. Mardia and Jupp (1999); Taghia et al. (2014). The VonMises distribution, parameterized by a mean μ and concentration κ is the natural extension of the normal distribution to the circle. For each von Mises component c_i in the mixture, we place a VonMises hyperprior on each μ_i, and a Gamma hyperprior on each κ_i, parameterized by shape $\hat{\alpha}$ and rate $\hat{\beta}$ parameters. The mixture weights w are selected from a Dirichlet prior with concentration parameters $\hat{a}_1, \ldots, \hat{a}_n$, fed into a Categorical prior to produce the latent component probabilities $m_1, \ldots, m_n$. Finally, the rotation angles are assumed iid from a Mixture of $c_1, \ldots, c_n$ weighted with $m_1, \ldots, m_n$.

Our model construction roughly follows that of Taghia et al. (2014) except that those authors choose to set the hyperprior μ_i concentration parameter as $\hat{\beta}\kappa_i$ with $\hat{\beta}$ a positive constant. We have experimented with both versions of the model and did not find any issues with identifiability using our construction on the examples we present later.

After observing p iid samples of the rotation angle $\phi_1^{\text{obs}}, \ldots, \phi_p^{\text{obs}}$, we condition the joint model for a specific number of mixtures n in eq. (19) on data to form the Bayesian posterior $\theta^n \mid \phi_1^{\text{obs}}, \phi_2^{\text{obs}}, \ldots \phi_p^{\text{obs}}$. We generate samples from the posterior using the No-U-Turn Sampler (NUTS) (Hoffman and Gelman 2014), a gradient-based Hamiltonian Monte Carlo (HMC) method (Duane et al. 1987; Neal 1996). In our

numerical computations we use the parameterizations as defined in the probabilistic programming language NumPyro (Phan et al. 2019; Rønning et al. 2021).

Later, we will calibrate models with varying number of mixtures n to the observed rotation angle data. Consequently it will be necessary to select the number of mixtures that best represents the underlying data, while remaining conservative. This model selection problem can be tackled via a number of approaches, e.g. information theoretic approaches (Akaike 1998; Spiegelhalter et al. 2002; van der Linde 2005; Watanabe and Opper 2010), Bayes factors (Friel and Pettitt 2008) and cross-validation (CV) (Vehtari et al. 2017). Please see Gelman et al. (2014); Watanabe (2021); Zhang et al. (2023) for the relative merits of these different approaches.

In this study we use a CV approach, specifically Leave-one-out cross-validation (LOOCV) as described in (Vehtari et al. 2017) via the implementation in ArviZ (Kumar et al. 2019), a Python package for exploratory data analysis. LOOCV is widely used to obtain a reliable test for model performance estimation and less commonly used as a model selection criterion. Although LOOCV is significantly more computationally expensive than information theoretic approaches such as Akaike information criterion (AIC) (Akaike 1998) and deviance information criteria (DIC) (Spiegelhalter et al. 2002; van der Linde 2005), LOOCV offers greater flexibility and applicability to complex models like the mixture model we consider here (Vehtari et al. 2015, 2017).

3.4 Eigenvalue model

We model the eigenvalues as log-normal random variables

$$\lambda_x \sim \text{Lognorm}(\hat{\mu}_x, \hat{\sigma}_x^2), \tag{20a}$$

$$\lambda_y \sim \text{Lognorm}(\hat{\mu}_y, \hat{\sigma}_y^2). \tag{20b}$$

This representation ensures positivity thus guaranteeing $\Lambda \in \text{Diag}^+(2)$. [2]

The simplicity of the model and the available data allow us to calibrate our model with Heilweil and Hsieh (2006) by calibrating the four parameters $(\hat{\mu}_x, \hat{\sigma}_x^2, \hat{\mu}_y, \hat{\sigma}_y^2)$ manually. In the presence of richer data more complex models could be developed and formally calibrated using e.g. MLE or Bayesian approaches.

3.5 Anisotropic hydraulic conductivity model

Following the arguments in Shivanand et al. (2024), we extend the construction of k in eqs. (14) and (18) to the stochastic setting. We treat k as a function of the random variable $\omega := (\phi, \lambda_x, \lambda_y)$ composed of the rotation angle and eigenvalues, i.e.

$$k(\omega) : \mathbb{S}^1 \times \mathbb{R}_*^+ \times \mathbb{R}_*^+ \to \text{Sym}^+(2), \tag{21}$$

on a probability space (triple) defined in the standard way, see e.g. Klenke (2020).

[2] In Shivanand et al. (2024) precisely the same construction is derived via $\text{Diag}^+(2)$ having Lie algebra $\mathfrak{Diag}(2)$ and modeling $\log(\Lambda) \in \mathfrak{Diag}(2)$ with the two diagonal entries modeled as two normal random variables.

We now discuss the full stochastic extension of eq. (14) and two special cases (Shivanand et al. 2024). In the full model, we will generate AHC tensors with randomness in both scaling and rotation

$$k(\omega) = R(\phi)\widehat{Q}\Lambda(\lambda_x, \lambda_y)\widehat{Q}^T R(\phi)^T. \tag{22}$$

In the first simplified model k_s we assume that ϕ is known perfectly and there is no rotation, i.e. $\hat{\phi} = 0$ and $R = I$. This means that the scaling is the only parameter that is varied, leading to

$$k_s(\omega) = \widehat{Q}\Lambda(\lambda_x, \lambda_y)\widehat{Q}^T. \tag{23}$$

In the second simplified model k_r we assume that both $\lambda_x = \hat{\lambda}_x$ and $\lambda_y = \hat{\lambda}_y$ are perfectly known, leading to randomness only in the rotations

$$k_r(\omega) = R(\phi)\widehat{Q}\widehat{\Lambda}(\hat{\lambda}_x, \hat{\lambda}_y)\widehat{Q}^T R(\phi)^T. \tag{24}$$

To produce samples $\{k(\omega_i)\}_{i=1}^N$ distributed according to k in eqs. (21) and (22), we first generate rotation angle samples assumed iid $\{\phi_i\}_{i=1}^N$ according to the posterior predictive distribution $\phi \mid \phi_1^{\text{obs}}, \ldots, \phi_p^{\text{obs}}$ (Gelman et al. 2020, Section 6.1) induced by the model eq. (19) at fixed n. We then generate eigenvalue samples $\{\lambda_x\}_{i=1}^N$ and $\{\lambda_y\}_{i=1}^N$ using a standard generator for the log-normal distribution, before finally passing each $\omega_i = (\phi_i, \lambda_{xi}, \lambda_{yi})$ through equation eq. (22). The process for generating samples from the models with fixed parameters eqs. (23) and (24) will be described in the following section.

3.6 Forward uncertainty propagation

To study how uncertainty in the AHC tensor induces uncertainty in the LOS surface displacement we calculate summary statistics of the LOS surface displacement using the Monte Carlo technique. Given N assumed iid samples $\{k_i\}_{i=1}^N$ we can calculate N solutions of $\{u_{\text{LOS}}(x, t, k_i)\}_{i=1}^N$ by solving the PDE system eq. (1) and calculating the LOS displacement eq. (4). The mean of the LOS displacement is then computed as

$$\mu(u_{\text{LOS}}(x,t)) := \frac{1}{N}\sum_{i=1}^{N} u_{\text{LOS}}(x, t, k_i), \tag{25}$$

and the unbiased estimation of standard deviation is calculated as

$$\text{Std}(u_{\text{LOS}}(x,t)) := \left[\frac{1}{N-1}\sum_{i=1}^{N}\left[u_{\text{LOS}}(x,t,k_i) - \mu(u_{\text{LOS}}(x,t))\right]^2\right]^{1/2}. \tag{26}$$

4 Results

We apply the methodology described in section 3 to develop two models reflecting different states of subjective Bayesian belief (Jaynes 2003) about the Anderson Junction site.

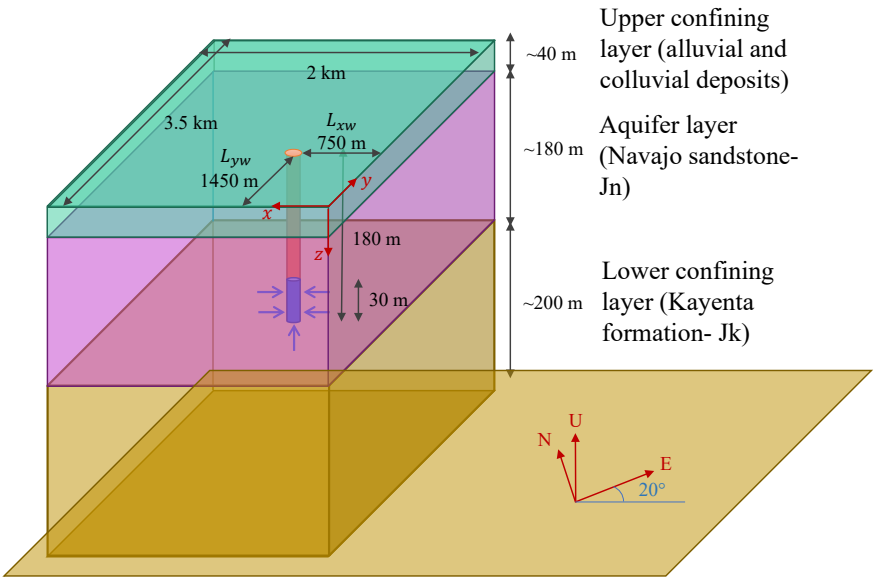

Fig. 5: Simplified conceptual model of the Anderson Junction aquifer system highlighting the dimensions, formations, and thicknesses of the layers within the cross-section. The figure also illustrates the model coordinate system in relation to the ENU global coordinate system. The domain is not to scale. Used under CC BY 4.0 license from Salehian Ghamsari et al. (2025).

In the first scenario, detailed in sections 4.1 to 4.5 we use the fracture data fig. 1 and the major and minor hydraulic conductivity estimates from the pump test in Heilweil and Hsieh (2006). Since the pump test determined the major principal direction of AHC using Papadopulus method, the rotation angle ϕ cannot lie along the fracture mode coinciding with well B. Consequently we construct a model that captures the complexity in the rotation angle data only in the direction of well A.

In the second scenario, described briefly in section 4.6, we assume no knowledge of the outcome of the pump test. Instead we rely solely on the fracture data and the general understanding that the hydraulic conductivity may be anisotropic – this is the same state of knowledge as in Heilweil and Hsieh (2006) *prior* to the pump test. Without the pump test data, the major principal direction remains uncertain and could be aligned with either of the primary fracture directions in fig. 1.

4.1 Specification of the poroelastic finite element model

Figure 5 shows the areal extent, formations, and thicknesses of layers in the model cross-section. The resulting three-dimensional mesh for finite element analysis fig. 6 represents three layers of the aquifer system. Figure 6 shows the positions of pumping and observation wells, and lines xx' and yy' are aligned with the x and y directions in fig. 1.

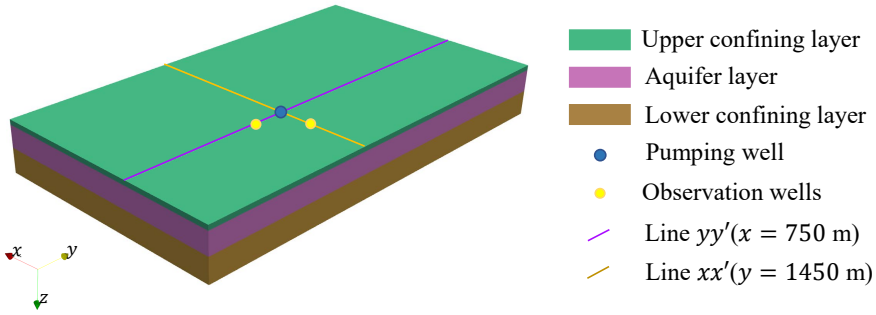

Fig. 6: Generated 3D mesh of the aquifer system illustrating the three layers. The figure also highlights the positions of the pumping and observation wells, as well as lines xx' and yy'. Used under CC BY 4.0 license from Salehian Ghamsari et al. (2025).

Description	Symbol	Unit	Value
Fluid source	f_p	s^{-1}	0.0
Body force	f_u	$\mathrm{N\,m}^{-3}$	0.0
Specific weight of water	ρg	$\mathrm{N\,m}^{-3}$	9807
Pumping rate	P_r	$\mathrm{m}^3\,\mathrm{s}^{-1}$	0.28
Extraction rate	g_p	$\mathrm{m\,s}^{-1}$	7.6×10^{-3}
Pumping duration	T_p	d	8
Incidence angle	θ	deg	43.86
Satellite heading angle	α_h	deg	15.0

Table 2: Model parameters. Used under CC BY 4.0 license from Salehian Ghamsari et al. (2025).

The model and layer parameters used in the finite element poroelastic model are presented in table 2 and table 3, respectively.

The boundary conditions on the variables (u, p, q) are displayed in table 4 and fig. 7 shows the boundaries used in the table.

More detailed justifications for these choices can be found in Salehian Ghamsari et al. (2025).

4.2 Calibrating the rotation angle model

Following the developments in section 3.3 we calibrate the rotation angle model eq. (19) for $n = 1, 2, 3$ mixtures against the fracture direction isolated around the direction of well A in fig. 1. This leads to three calibrated models denoted VM1, VM2 and VM3.

Because fracture orientation data at the Anderson junction site is only available in summarized form fig. 1, rather than raw rotation angle data $\{\phi_i^{\mathrm{obs}}\}_{i=1}^{M}$, we generate $M = 1000$ synthetic rotation angle observations for use in the calibration. Our methodology is not limited to this setting and works well with raw rotation angle data.

Description	Symbol	Unit	Upper conf.	Aquifer	Lower conf.
Porosity	ϕ	-	10%	32%	8%
Biot coefficient	α	-	0.868	0.998	0.858
Specific storage	S_ϵ	Pa^{-1}	0.8×10^{-10}	1.5×10^{-10}	0.8×10^{-10}
Shear modulus	μ_s	Pa	7.7×10^{9}	5.06×10^{9}	7.9×10^{9}
Lame's first parameter	λ	Pa	6.088×10^{9}	3.768×10^{9}	6.156×10^{9}
Hydraulic conductivity xx	k_{xx}	$\mathrm{m}^3\,\mathrm{s}\,\mathrm{kg}^{-1}$	5×10^{-12}	1.1×10^{-8}	5×10^{-12}
Hydraulic conductivity yy	k_{yy}	$\mathrm{m}^3\,\mathrm{s}\,\mathrm{kg}^{-1}$	5×10^{-12}	4.7×10^{-10}	5×10^{-12}
Hydraulic conductivity zz	k_{zz}	$\mathrm{m}^3\,\mathrm{s}\,\mathrm{kg}^{-1}$	5×10^{-12}	5×10^{-7}	5×10^{-12}

Table 3: Material parameters of the layers. Used under CC BY 4.0 license from Salehian Ghamsari et al. (2025).

	Boundary condition	Boundary
Fluid problem (q, p)	$q \cdot n = 0$	$\Gamma_b \cup \Gamma_{sx} \cup \Gamma_{sy} \cup \Gamma_t$
	$q \cdot n = g_p$	Γ_{pw}
	$q \cdot n = 0$	Γ_w
Solid problem (u)	$u = 0$	Γ_b
	$u_x = 0$	Γ_{sx}
	$u_y = 0$	Γ_{sy}
	$\sigma \cdot n = 0$	$\Gamma_t \cup \Gamma_{pw}$
	$u \cdot n = 0$	Γ_w

Table 4: Boundary conditions of fluid and solid problem. Used under CC BY 4.0 license from Salehian Ghamsari et al. (2025).

Symbol	Description	Unit	Value
$\hat{\mu}$	measure of location	rad	0.0
$\hat{\kappa}$	measure of concentration	rad^{-2}	π
$\hat{\alpha}$	shape parameter	-	20.0
$\hat{\beta}$	rate parameter	rad^2	0.1
$\hat{a}_1, \ldots, \hat{a}_n$	concentration parameters	-	$1, 1, ..., 1.$

Table 5: Non-informative prior parameters for the rotation angle model.

The posterior predictive distributions of the three calibrated models are shown in fig. 8. The blue histogram summarizes the posterior predictive rotation angle data, and the green histogram summarizes the rotation angle data used for calibration. 2VM and 3VM show a reasonable fit to the original data, while 1VM is, as expected, inadequate.

In table 6 we show the results of the model selection. The models are ranked from best to worst based on the `elpd_loo` – a higher `elpd_loo` indicates a better out-of-sample predictive fit. The estimated effective number of parameters `p_loo` reflects the

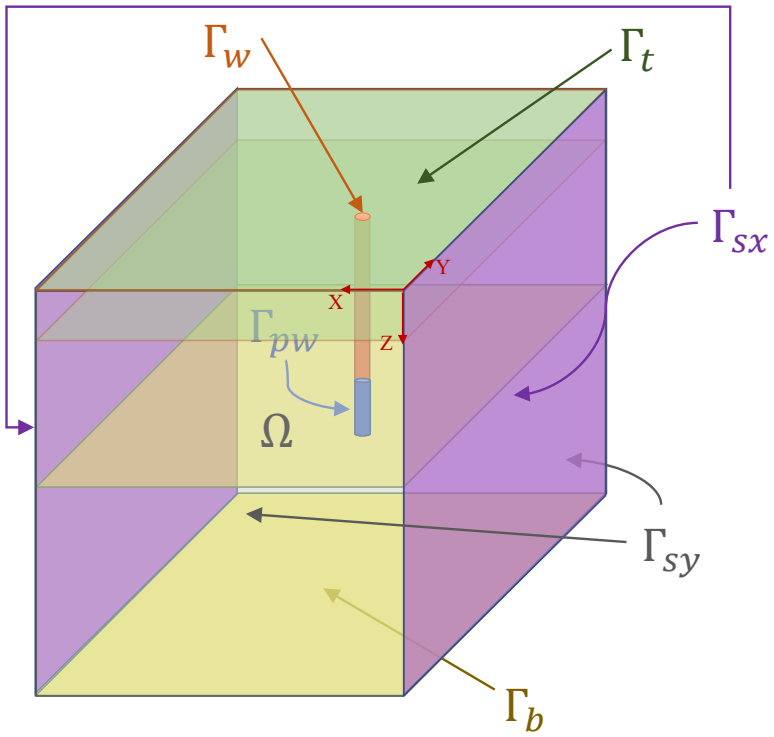

Fig. 7: Aquifer model illustrating the domain and defined boundaries referenced in the table 4, the domain is not to scale. Used under CC BY 4.0 license from Salehian Ghamsari et al. (2025).

complexity of the model – a higher value indicating greater complexity. Following the guidelines in Vehtari et al. (2017), a model can be considered better than another only if the `elpd_diff` significantly exceeds the standard error `SE` of the ELPD estimate. The `elpd_diff` between 2VM and 3VM is 15.99, which is less than the standard error of 21.52, so we cannot conclude that 3VM is superior to 2VM. We then compare the complexity using `p_loo` and determine that 2VM is less complex than 3VM - consequently we choose 2VM and continue with 2VM through the following sections.

4.3 Calibrating the eigenvalue model

We calibrate the four parameters $(\hat{\mu}_x, \hat{\mu}_y, \hat{\sigma}_x^2, \hat{\sigma}_y^2)$ of the stochastic model of the eigenvalues eq. (20). As data we use the inferred values of the AHC $k_{xx} \pm 21\%$ and $k_{yy} \pm 19\%$ reported in Heilweil and Hsieh (2006) which corresponds to an anisotropy ratio of approximately 24 to 1. The values of k_{xx} and k_{yy} are provided in table 3. In the original study no precise meaning is attached to the quoted $\pm$ statistic, so we choose to interpret this to mean that approximately 98 % of the probability mass of the Lognorm should lie between the $\pm$ limits. We set $\hat{\mu}_x = k_{xx}$, $\hat{\mu}_y = k_{yy}$ and iteratively adjust the

Model	rank	elpd_loo	p_loo	elpd_diff	SE
3VM	1	276.80	23.41	0.00	20.63
2VM	2	260.81	4.95	15.99	21.52
1VM	3	44.48	1.41	232.32	13.98

Table 6: Model selection results. `rank`: The rank-order of the models based on `elpd_loo`. `elpd_loo`: Expected log pointwise predictive density. `p_loo`: Estimated effective number of parameters. `elpd_diff`: The difference in expected log pointwise predictive density (ELPD) between models, computed relative to the top-ranked model, which always has an `elpd_diff` of 0. SE: Standard error of the ELPD estimate. 2VM is the preferred model; interpretation of the results is given in the text.

variance. We find that $\hat{\sigma}_x^2 = \hat{\sigma}_y^2 = 0.0064$ approximately satisfies the 98 % condition. The PDF with these parameters are shown in fig. 9.

4.4 Generation of AHC tensors

Using the calibrated models in sections 4.2 and 4.3 we generate stochastic AHC tensors via eqs. (22) to (24). Figure 10 provides a visualization of the random samples of the three different AHC models. The elliptical shape of the AHC tensor illustrates both the direction and magnitude of AHC along the principal directions. The direction of the ellipses indicates the principal major and minor directions of hydraulic conductivity, while the radii represent the magnitude of hydraulic conductivity in those principal directions.

4.5 Forward uncertainty analysis

For each case eqs. (22) to (24) we generate $N = 8000$ samples of the AHC tensor and propagate this uncertainty through the PDE model of the Anderson Junction. The evaluation of the model at each sample takes around 10 min on 32 MPI processes on the aion High-Performance Computing (HPC) at the University of Luxembourg (Varrette et al. 2022). We execute 128 evaluations simultaneously across the HPC using GNU Parallel (Tange 2024). For each evaluation line-of-sight displacement u_{LOS} on the top surface Γ_t is written out to disk (around 35 MB) in the ADIOS2 format using adios4dolfinx (Dokken 2024). The data is read back in on a single HPC job with 8 MPI processes to compute summary statistics eqs. (25) and (26).

As a baseline for comparison in fig. 11, we show the deterministic Anderson Junction hypothetical intermediate pumping scenario with rate $4 \times P_r$ after 8 d duration from (Salehian Ghamsari et al. 2025). We remind the reader the effect of the LOS

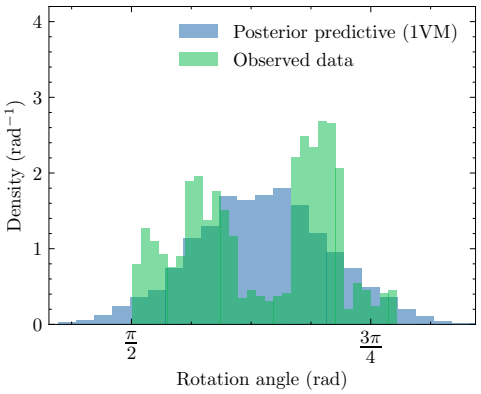

(a) Posterior predictive distribution of 1VM.

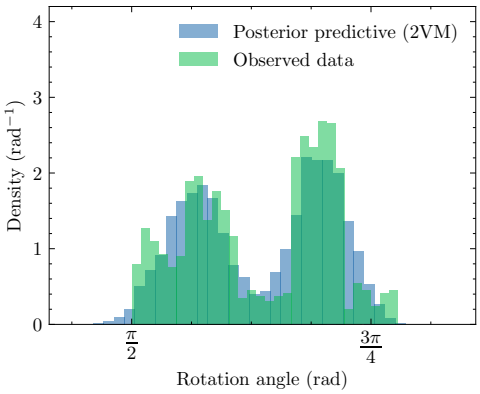

(b) Posterior predictive distribution of 2VM.

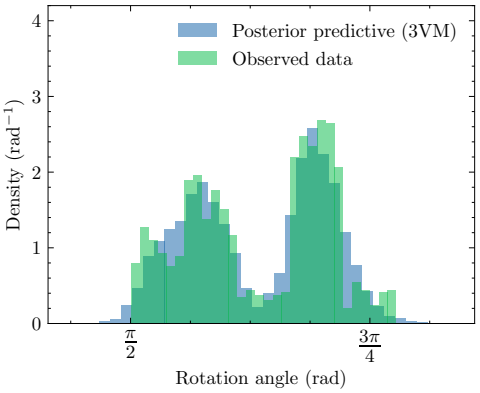

(c) Posterior predictive distribution of mixture of 3VM.

Fig. 8: Posterior predictive checks: posterior predictive (green) and original training data (blue).

perspective in the outputs, which 'shifts' the observed displacement towards the east-south of the pumping well as the satellite is positioned to the west-north of the aquifer.

In fig. 13, we present the mean and standard deviation of LOS displacement calculated using AHC with random scaling alone. The mean fig. 13a closely resembles the LOS displacement predicted at Anderson Junction using the hypothetical intermediate pumping test scenario (fig. 11). The standard deviation indicates a very slight variation along a band aligned with the major principal direction.

Figure 14 shows the mean and standard deviation of the LOS displacement with random rotation applied. The results are similar to those observed in the random scaling and rotation scenario, implying that the randomness in rotation, induced by

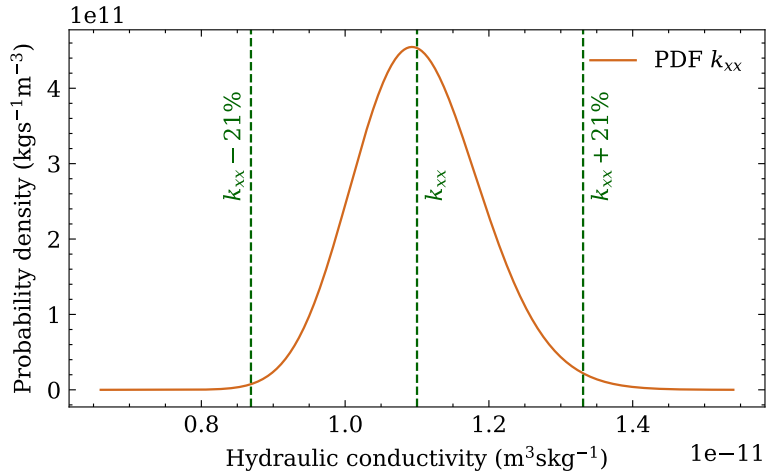

(a) Distribution of AHC magnitude in major axis.

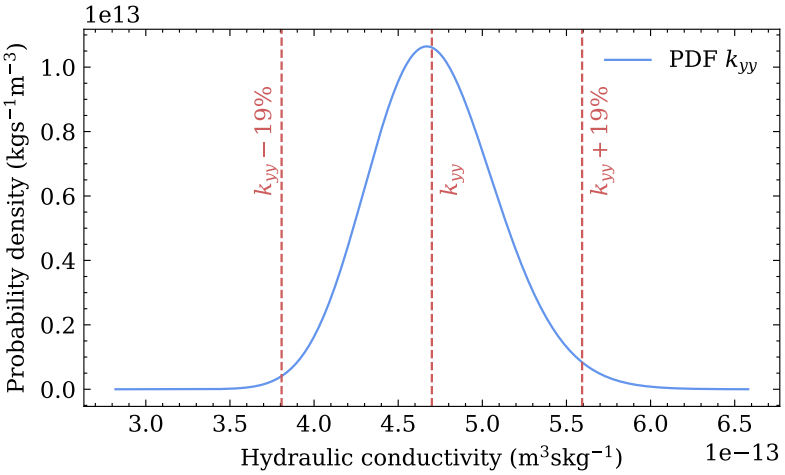

(b) Distribution of AHC magnitude in minor axis.

Fig. 9: Probability density functions of the two eigenvalues.

the structural geological data, has the dominant effect on the line-of-sight displacement here.

4.6 Second scenario

In this second modeling scenario, we assume that the AHC (from Heilweil and Hsieh (2006)) is unknown. Consequently the major principal direction could be coincident with either of the fracture modes fig. 1. The lack of knowledge of the pump test also

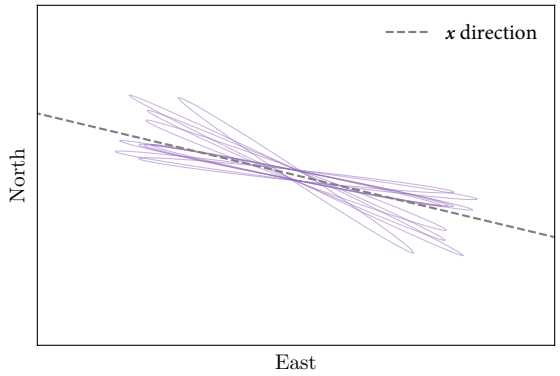

(a) Samples from scaling and rotation model eq. (22).

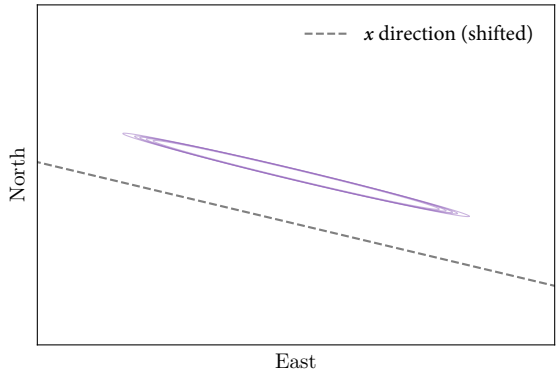

(b) Samples from scaling model eq. (23). Line in x direction is shifted by a constant translation for easier visualization.

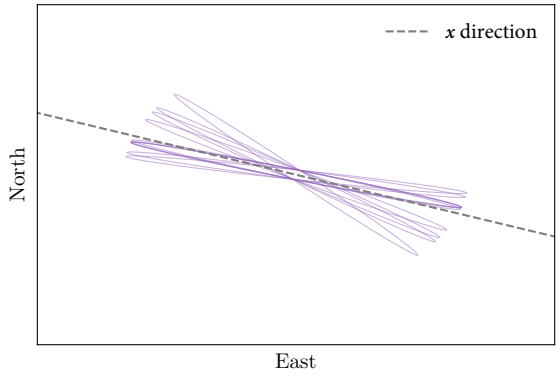

(c) Samples from rotation model eq. (24).

Fig. 10: Visualization of random samples from three models for stochastic AHC. Each random sample is plotted as an ellipse with the direction of the ellipse representing the principal directions and the radii representing the magnitude of the hydraulic conductivity in the principal directions.

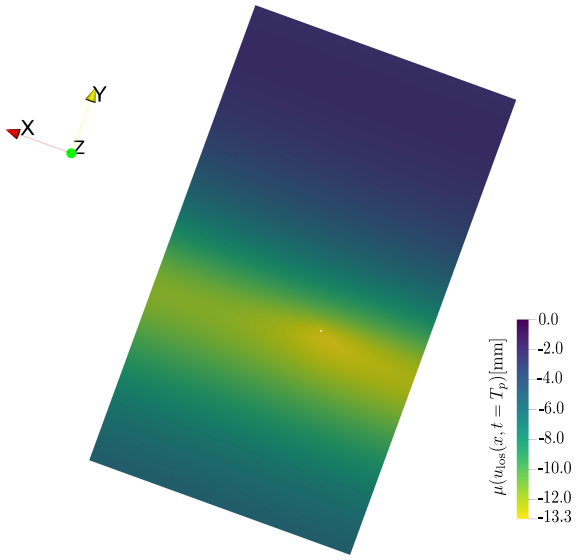

Fig. 11: Simulated LOS surface displacement at the end of pumping for an hypothetical intermediate pumping with $4 \times P_r$ and 8 d duration. Used under CC BY 4.0 license from Salehian Ghamsari et al. (2025).

means that we need to express a greater degree of uncertainty about the anisotropy ratio between the principle directions.

Because of the additional mode to account for in the fracture data, we choose to calibrate 3VM and a new richer 4VM model for the rotation angle - the model selection process (full results not shown) selects 4VM. The posterior predictive distribution of this mixture model is shown in fig. 15a.

Using eq. (20), we generate eigenvalues applying a higher standard deviation, which leads to a anisotropy ratio from around 1:9 to 1:1. We then generate random AHC tensors with random scaling and rotation using eq. (22). The elliptical shape of these random AHC tensors is shown in fig. 15b. We can see that our parameterization using a multi-modal angle model and two eigenvectors can represent that the major principal direction could lie in the direction of either well A or well B.

Finally, we quantify AHC uncertainty in the LOS displacement outputs by solving our poroelastic finite element model for the generated random AHC tensors. A few sample LOS displacement outputs are presented in fig. 15c, illustrating the variability in responses due to different AHC orientations and magnitudes. We remark how the mean shown in fig. 15d exhibits an almost circular shape due to the AHC tensors having major direction approximately oriented along the direction of either well A or B.

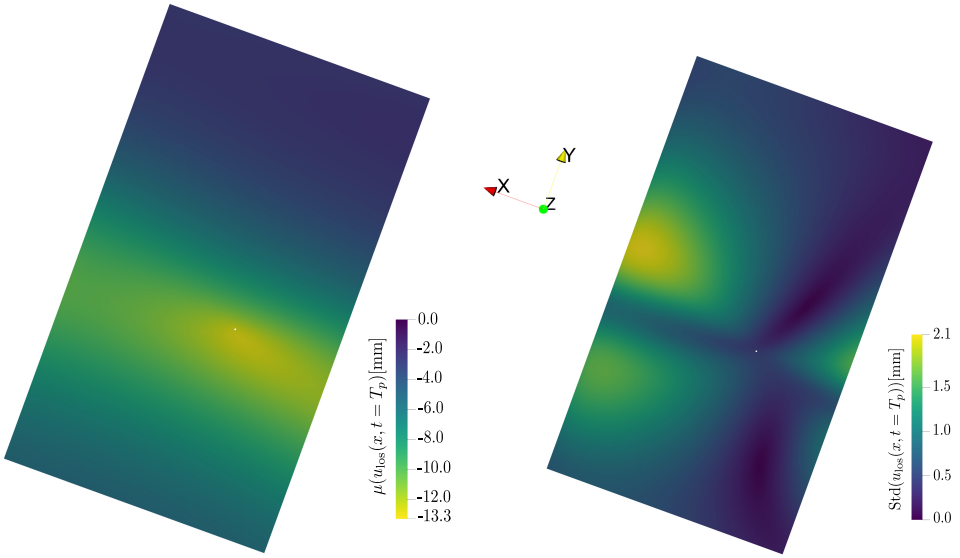

(a) Mean of LOS displacement (random scaling and rotation AHC).

(b) Standard deviation of LOS displacement (random scaling and rotation AHC).

Fig. 12: Mean and standard deviation of the LOS displacement outputs from executing the poroelastic model using AHC with randomness in both scaling and rotation. T_p is the time when the pumping finished after 8 d of pumping. The mean values are truncated at zero from above.

5 Conclusions

In this study we presented a novel random model of AHC that can incorporate uncertain structural data. The model consists of three components; a Bayesian rotation angle model built from a mixture of circular von Mises distributions that encodes the principal direction of AHC, a model for positive eigenvalues that controls the magnitude of the AHC in the principal directions, both feeding into a Lie group construction for the AHC tensor. Our goal has been to design a model that could serve as a prior in a Bayesian inference setting where InSAR-derived line-of-sight data contain information about AHC. By calibrating the model against observed fracture orientations and pump test data from Anderson Junction, we were able to define two conceptual states of belief about the site. Our results show that the methodology provides a flexible tool for modeling uncertainty and that uncertainty in the AHC orientation has a larger impact on the LOS InSAR displacement predictions than the magnitudes of the principal directions.

In the future, we plan to explore the Bayesian calibration of the full model against real and synthetic InSAR data in order to explore parameter identifiability. The computational burden of the PDE solver presents some technological challenges. In particular, to minimise the number of model evaluations needed to create a Markov

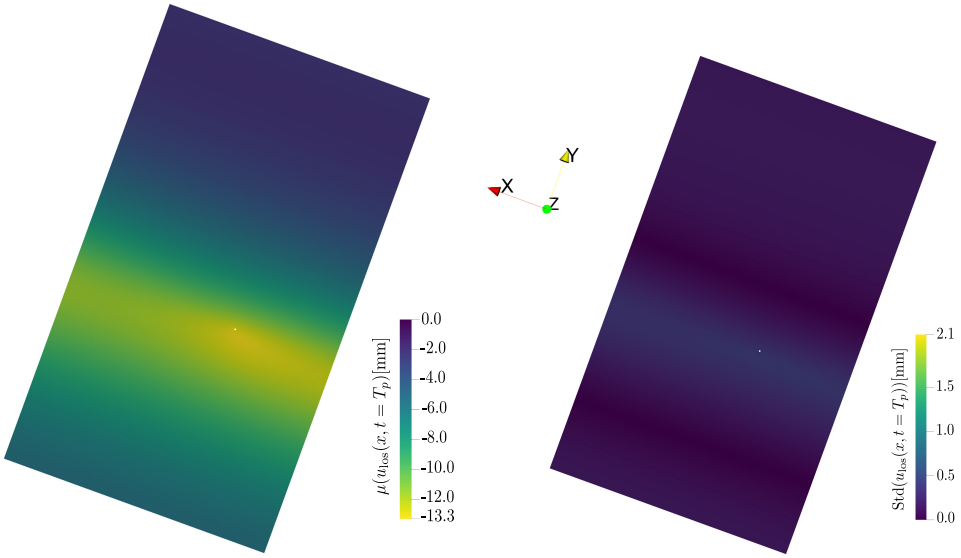

(a) Mean of LOS displacement (random scaling AHC).

(b) Standard deviation of LOS displacement (random scaling AHC).

Fig. 13: Mean and standard deviation of the LOS displacement outputs from executing the poroelastic model using AHC with randomness in scaling. The mean values are truncated at zero from above.

chain on the posterior we need to use a gradient-based sampling algorithm, e.g. NUTS, which requires the derivative of the log-posterior with respect to the model parameters. This can be calculated efficiently via the adjoint (back-propagation) technique. However, our full model is constructed from a complex mixture of NumPyro (probabilistic) and DOLFINx (PDE) components and although we can derive the adjoint model of each part individually and automatically using NumPyro/JAX (Phan et al. 2019; Bradbury et al. 2018) and pyadjoint (Mitusch et al. 2019), we are not currently able to write a NumPyro model containing a DOLFINx PDE solve and then derive the corresponding adjoint model. Some recent work (Bouziani and Ham 2023) show coupling of PDE and machine-learning model graphs for gradient calculation and this technique could be adapted to our model.

Supplementary material. The supplementary material (Salehian Ghamsari and Hale 2024a) includes input data, full code and further mathematical details of the finite element model.

Acknowledgments. We would like to thank Guendalina Palmirotta and Damian Mingo Ndiwago for their valuable comments on circular statistics and model selection, respectively.

The experiments presented in this paper were carried out using the HPC facilities of the University of Luxembourg (Varrette et al. 2022).

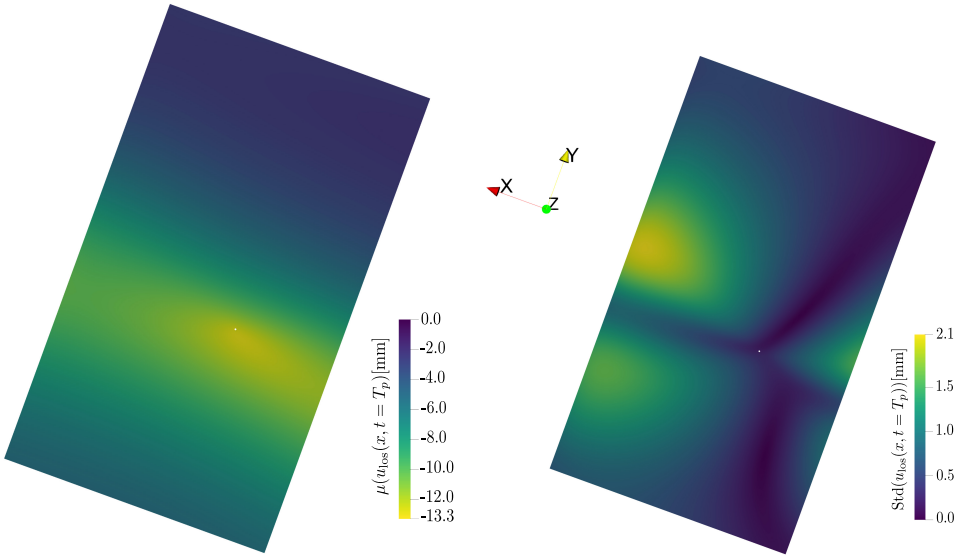

(a) Mean of LOS displacement (random rotation AHC).

(b) Standard deviation of LOS displacement (random rotation AHC).

Fig. 14: Mean and standard deviation of the LOS displacement outputs from executing the poroelastic model using AHC with randomness in rotation. The very small mean values are truncated at zero from above.

Funding. This work was funded in whole, or in part, by the Luxembourg National Research Fund (FNR), grant reference PRIDE/17/12252781. For the purposes of open access, and in fulfilment of the obligations arising from the grant agreement, the authors have applied a Creative Commons Attribution 4.0 International (CC BY 4.0) license to any Author Accepted Manuscript version arising from this submission.

Competing interests. The authors have no relevant financial or non-financial interests to disclose.

Authorship statement. SSG: Data curation, Methodology, Software, Formal analysis, Investigation, Writing - Original Draft, Validation, Visualization. TvD: Writing - Review & Editing, Funding acquisition, Supervision. JSH: Conceptualization, Methodology, Software, Investigation, Writing - Original Draft, Writing - Review & Editing, Funding acquisition, Project administration, Supervision.

References

Alghamdi, A., Hesse, M.A., Chen, J., Villa, U., Ghattas, O.: Bayesian Poroelastic Aquifer Characterization From InSAR Surface Deformation Data. 2. Quantifying

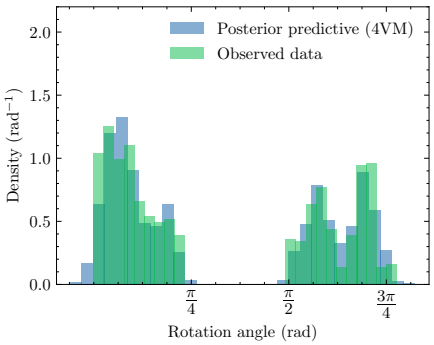

(a) Posterior predictive distribution of mixture of four von Mises model.

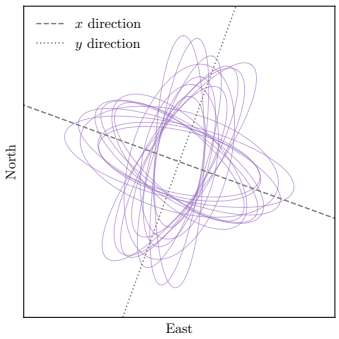

(b) AHC tensor with randomness in scaling and rotation.

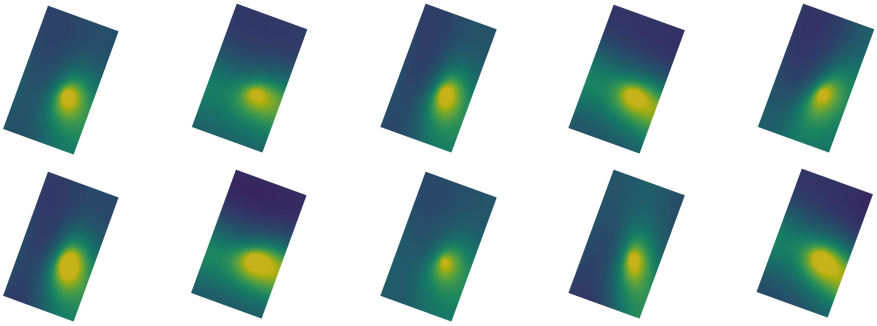

(c) Samples of LOS displacement.

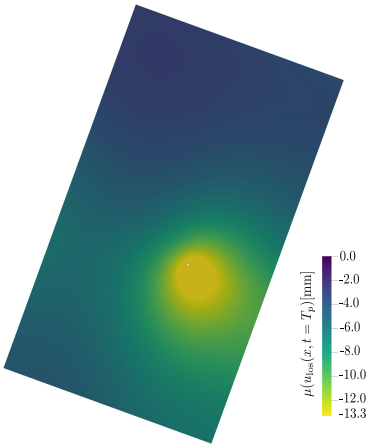

(d) Mean of LOS displacement.

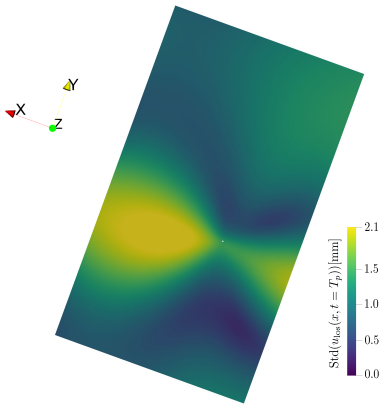

(e) Standard deviation of LOS displacement.

Fig. 15: Results of second scenario. The scale and unit for samples fig. 15c is the same as the mean fig. 15d.

the Uncertainty. Water Resources Research **57**(11), 2021–029775 (2021) https://doi.org/10.1029/2021WR029775

Alghamdi, A., Hesse, M.A., Chen, J., Ghattas, O.: Bayesian Poroelastic Aquifer Characterization From InSAR Surface Deformation Data. Part I: Maximum A Posteriori Estimate. Water Resources Research **56**(10), 2020–027391 (2020) https://doi.org/10.1029/2020WR027391

Alghamdi, A., Hesse, M.A., Chen, J., Ghattas, O.: Advancing aquifer characterization through the integration of satellite geodesy, geomechanics, and bayesian inference. Authorea Preprints (2024) https://doi.org/10.22541/essoar.172988076.62528060/v1

Akaike, H.: Information theory and an extension of the maximum likelihood principle. In: Selected Papers of Hirotugu Akaike, pp. 199–213. Springer, New York (1998). https://doi.org/10.1007/978-1-4612-1694-0_15

Alghamdi, A.: Bayesian inverse problems for quasi-static poroelasticity with application to ground water aquifer characterization from geodetic data. Thesis, University of Texas at Austin (May 2020). https://doi.org/10.26153/tsw/13182

Alnaes, M.S., Logg, A., Olgaard, K.B., Rognes, M.E., Wells, G.N.: Unified form language: A domain-specific language for weak formulations of partial differential equations. ACM Trans. Math. Softw. **40**(2) (2014) https://doi.org/10.1145/2566630

Amitrano, D., Martino, G.D., Iodice, A., Mitidieri, F., Papa, M.N., Riccio, D., Ruello, G.: Sentinel-1 for monitoring reservoirs: A performance analysis. Remote Sensing **6**(11), 10676–10693 (2014) https://doi.org/10.3390/rs61110676

Adler, P.M., Thovert, J.-F.: Fractures and Fracture Networks. Theory and Applications of Transport in Porous Media, vol. 15. Springer, Dordrecht (1999). https://doi.org/10.1007/978-94-017-1599-7

Axler, S.: Linear Algebra Done Right. Undergraduate Texts in Mathematics. Springer, New York (2024). https://doi.org/10.1007/978-3-031-41026-0

Baratta, I.A., Dean, J.P., Dokken, J.S., Habera, M., Hale, J.S., Richardson, C.N., Rognes, M.E., Scroggs, M.W., Sime, N., Wells., G.N.: DOLFINx: The next generation FEniCS problem solving environment. Zenodo (2023) https://doi.org/10.5281/zenodo.10447666

Berre, I., Doster, F., Keilegavlen, E.: Flow in Fractured Porous Media: A Review of Conceptual Models and Discretization Approaches. Transport in Porous Media **130**(1), 215–236 (2019) https://doi.org/10.1007/s11242-018-1171-6

Bradbury, J., Frostig, R., Hawkins, P., Johnson, M.J., Leary, C., Maclaurin, D., Necula,

G., Paszke, A., VanderPlas, J., Wanderman-Milne, S., Zhang, Q.: JAX: Composable Transformations of Python+NumPy programs. http://github.com/jax-ml/jax

Bouziani, N., Ham, D.A.: Physics-driven machine learning models coupling PyTorch and Firedrake. In: ICLR 2023 Workshop on Physics for Machine Learning (2023). https://doi.org/10.48550/arXiv.2303.06871

Bishop, C.M.: Pattern Recognition and Machine Learning, 1st edn. Information Science and Statistics. Springer, New York (2006)

Blei, D.M., Kucukelbir, A., McAuliffe, J.D.: Variational Inference: A Review for Statisticians. Journal of the American Statistical Association **112**(518), 859–877 (2017) https://doi.org/10.1080/01621459.2017.1285773

Brenner, S.C., Scott, L.R.: The Mathematical Theory of Finite Element Methods. Texts in Applied Mathematics, vol. 15. Springer, New York, NY (2008). https://doi.org/10.1007/978-0-387-75934-0

Burbey, T.J.: Three-dimensional deformation and strain induced by municipal pumping, Part 2: Numerical analysis. Journal of Hydrology **330**(3), 422–434 (2006) https://doi.org/10.1016/j.jhydrol.2006.03.035

Basu, N.B., Van Meter, K.: 4.3 - Sustainability of Groundwater Resources. In: Ahuja, S. (ed.) Comprehensive Water Quality and Purification, pp. 57–75. Elsevier, Waltham (2014). https://doi.org/10.1016/B978-0-12-382182-9.00062-1

Burbey, T.J., Warner, S.M., Blewitt, G., Bell, J.W., Hill, E.: Three-dimensional deformation and strain induced by municipal pumping, part 1: Analysis of field data. Journal of Hydrology **319**(1), 123–142 (2006) https://doi.org/10.1016/j.jhydrol.2005.06.028

Caretta, M.A., Mukherji, A., Arfanuzzaman, M., Betts, R.A., Gelfan, A., Hirabayashi, Y., Lissner, T.K., Liu, J., Gunn, E.L., Morgan, R., Mwanga, S., Supratid, S.: Water. In: Climate Change 2022: Impacts, Adaptation and Vulnerability. Technical report, Cambridge University Press, Cambridge, UK and New York, NY, USA (2022). https://doi.org/10.1017/9781009325844.006

Davis, J.C.: Statistics and Data Analysis in Geology, 3rd edn., p. 656. Wiley, New York (2002)

Duane, S., Kennedy, A.D., Pendleton, B.J., Roweth, D.: Hybrid Monte Carlo. Physics Letters B **195**(2), 216–222 (1987) https://doi.org/10.1016/0370-2693(87)91197-X

Dokken, J.S.: ADIOS4DOLFINx: A framework for checkpointing in FEniCS. Journal of Open Source Software **9**(96), 6451 (2024) https://doi.org/10.21105/joss.06451

Ferronato, M., Castelletto, N., Gambolati, G.: A fully coupled 3-D mixed finite element

model of Biot consolidation. Journal of Computational Physics **229**(12), 4813–4830 (2010) https://doi.org/10.1016/j.jcp.2010.03.018

Fuhrmann, T., Garthwaite, M.C.: Resolving Three-Dimensional Surface Motion with InSAR: Constraints from Multi-Geometry Data Fusion. Remote Sensing **11**(3), 241 (2019) https://doi.org/10.3390/rs11030241

Fernández-Martínez, J.L., Fernández-Muñiz, Z., Pallero, J.L.G., Pedruelo-González, L.M.: From Bayes to Tarantola: New insights to understand uncertainty in inverse problems. Journal of Applied Geophysics **98**, 62–72 (2013) https://doi.org/10.1016/j.jappgeo.2013.07.005

Food and Agriculture Organization of the United Nations (FAO): Water (2022). http://www.fao.org/water/en/ Accessed 2022-09-09

Friel, N., Pettitt, A.N.: Marginal Likelihood Estimation via Power Posteriors. Journal of the Royal Statistical Society Series B: Statistical Methodology **70**(3), 589–607 (2008) https://doi.org/10.1111/j.1467-9868.2007.00650.x . Accessed 2024-12-17

Galloway, D.L., Burbey, T.J.: Review: Regional land subsidence accompanying groundwater extraction. Hydrogeology Journal **19**(8), 1459–1486 (2011) https://doi.org/10.1007/s10040-011-0775-5

Gelman, A., Hwang, J., Vehtari, A.: Understanding predictive information criteria for bayesian models. Statistics and Computing **24**, 997–1016 (2014) https://doi.org/10.1007/s11222-013-9416-2

Guo, Q., Huang, J., Zhou, Z., Wang, J.: Experiment and Numerical Simulation of Seawater Intrusion under the Influences of Tidal Fluctuation and Groundwater Exploitation in Coastal Multilayered Aquifers. Geofluids (2019) https://doi.org/10.1155/2019/2316271

Guilleminot, J., Soize, C.: Stochastic modeling of anisotropy in multiscale analysis of heterogeneous materials: A comprehensive overview on random matrix approaches. Mechanics of Materials **44**(SI), 35–46 (2012) https://doi.org/10.1016/j.mechmat.2011.06.003

Guilleminot, J., Soize, C., Ghanem, R.G.: Stochastic representation for anisotropic permeability tensor random fields. International Journal for Numerical and Analytical Methods in Geomechanics **36**(13), 1592–1608 (2012) https://doi.org/10.1002/nag.1081

Gelman, A., Vehtari, A., Simpson, D., Margossian, C.C., Carpenter, B., Yao, Y., Kennedy, L., Gabry, J., Bürkner, P.-C., Modrák, M.: Bayesian Workflow. Technical report, arXiv (November 2020). https://doi.org/10.48550/arXiv.2011.01808

Hall, B.C.: Lie Groups, Lie Algebras, and Representations: An Elementary Introduction. Graduate Texts in Mathematics, vol. 222. Springer, Cham (2015). https://doi.org/10.1007/978-3-319-13467-3

Hoffman, M.D., Gelman, A.: The no-u-turn sampler: Adaptively setting path lengths in hamiltonian monte carlo. Journal of Machine Learning Research **15**(47), 1593–1623 (2014)

Heilweil, V.M., Hsieh, P.A.: Determining Anisotropic Transmissivity Using a Simplified Papadopulos Method. Groundwater **44**(5), 749–753 (2006) https://doi.org/10.1111/j.1745-6584.2006.00210.x

Hesse, M.A., Stadler, G.: Joint inversion in coupled quasi-static poroelasticity. Journal of Geophysical Research: Solid Earth **119**(2), 1425–1445 (2014) https://doi.org/10.1002/2013JB010272

Hurlow, H.A.: The Geology of the Central Virgin River Basin, Southwestern Utah, and Its Relation to Ground-water Conditions. Water-resources bulletin / Utah Geological Survey, vol. 26. Utah Geological Survey, Utah Dept. of Natural Resources, Salt Lake City, UT (1998). ISBN: 978-1-55791-614-3

Jaynes, E.T.: Probability Theory: The Logic of Science. Cambridge University Press, Cambridge, UK (2003). https://doi.org/10.1017/CBO9780511790423

Kumar, R., Carroll, C., Hartikainen, A., Martin, O.: ArviZ a unified library for exploratory analysis of Bayesian models in Python. Journal of Open Source Software **4**(33), 1143 (2019) https://doi.org/10.21105/joss.01143

Kirby, R.C., Logg, A.: A compiler for variational forms. ACM Trans. Math. Softw. **32**(3), 417–444 (2006) https://doi.org/10.1145/1163641.1163644

Klenke, A.: Probability Theory: A Comprehensive Course. Universitext. Springer, Cham (2020). https://doi.org/10.1007/978-3-030-56402-5

Lark, R., Clifford, D., Waters, C.: Modelling complex geological circular data with the projected normal distribution and mixtures of von Mises distributions. Solid Earth **5**(2), 631–639 (2014) https://doi.org/10.5194/se-5-631-2014

Ley, C., Verdebout, T.: Modern Directional Statistics. Chapman and Hall/CRC, New York (2017). https://doi.org/10.1201/9781315119472

Massonnet, D., Feigl, K.L.: Radar interferometry and its application to changes in the Earth's surface. Reviews of Geophysics **36**(4), 441–500 (1998) https://doi.org/10.1029/97RG03139

Mitusch, S.K., Funke, S.W., Dokken, J.S.: dolfin-adjoint 2018.1: automated adjoints for FEniCS and Firedrake. Journal of Open Source Software **4**(38), 1292 (2019)

https://doi.org/10.21105/joss.01292

Mardia, K.V., Jupp, P.E.: Directional Statistics. Wiley Series in Probability and Statistics. John Wiley & Sons, Ltd, West Sussex, UK (1999). https://onlinelibrary.wiley.com/doi/abs/10.1002/9780470316979.fmatter Accessed 2024-12-12

Mulder, K., Jongsma, P., Klugkist, I.: Bayesian inference for mixtures of von Mises distributions using reversible jump MCMC sampler. Journal of Statistical Computation and Simulation **90**(9), 1539–1556 (2020) https://doi.org/10.1080/00949655.2020.1740997

Mao, W., Mu, X., Zheng, Y., Yan, G.: Leave-one-out cross-validation-based model selection for multi-input multi-output support vector machine. Neural Computing and Applications **24**(2), 441–451 (2014) https://doi.org/10.1007/s00521-012-1234-5

Neal, R.M.: Monte Carlo Implementation. In: Bayesian Learning for Neural Networks, pp. 55–98. Springer, New York, NY (1996). https://doi.org/10.1007/978-1-4612-0745-0_3

Papadopulos, I.S.: Nonsteady flow to a well in an infinite anisotropic aquifer. In: Proceedings of the Symposium on Hydrology of Fractured Rocks (1965). https://unesdoc.unesco.org/ark:/48223/pf0000141973 Accessed 2024-04-17

Pollard, D.D., Fletcher, R.C.: Fundamentals of Structural Geology, (2005)

Pewsey, A., García-Portugués, E.: Recent advances in directional statistics. TEST **30**(1), 1–58 (2021) https://doi.org/10.1007/s11749-021-00759-x

Phan, D., Pradhan, N., Jankowiak, M.: Composable effects for flexible and accelerated probabilistic programming in numpyro. arXiv preprint arXiv:1912.11554 (2019)

Rad, N.N., Bekker, A., Arashi, M.: Enhancing wind direction prediction of South Africa wind energy hotspots with Bayesian mixture modeling. Scientific Reports **12**(1), 11442 (2022) https://doi.org/10.1038/s41598-022-14383-8

Rønning, O., Ley, C., Mardia, K.V., Hamelryck, T.: Time-efficient Bayesian Inference for a (Skewed) Von Mises Distribution on the Torus in a Deep Probabilistic Programming Language. In: 2021 IEEE International Conference on Multisensor Fusion and Integration for Intelligent Systems (MFI), pp. 1–8 (2021). https://doi.org/10.1109/MFI52462.2021.9591184 . https://ieeexplore.ieee.org/abstract/document/9591184

Spiegelhalter, D.J., Best, N.G., Carlin, B.P., Van Der Linde, A.: Bayesian Measures of Model Complexity and Fit. Journal of the Royal Statistical Society Series B: Statistical Methodology **64**(4), 583–639 (2002) https://doi.org/10.1111/1467-9868.00353

Scroggs, M.W., Baratta, I.A., Richardson, C.N., Wells, G.N.: Basix: A runtime finite element basis evaluation library. Journal of Open Source Software **7**(73), 3982 (2022) https://doi.org/10.21105/joss.03982

Scroggs, M.W., Dokken, J.S., Richardson, C.N., Wells, G.N.: Construction of arbitrary order finite element degree-of-freedom maps on polygonal and polyhedral cell meshes. ACM Trans. Math. Softw. **48**(2) (2022) https://doi.org/10.1145/3524456

Salehian Ghamsari, S., Hale, J.S.: Supplementary material for "A random model of anisotropic hydraulic conductivity tailored to the InSAR-based analysis of aquifers" (2024). https://doi.org/10.5281/zenodo.14170026

Salehian Ghamsari, S., Hale, J.S.: Supplementary material for "Can the anisotropic hydraulic conductivity of an aquifer be determined using surface displacement data? A case study" (2024). https://doi.org/10.5281/zenodo.10890121

Salehian Ghamsari, S., Dam, T., Hale, J.S.: Can the anisotropic hydraulic conductivity of an aquifer be determined using surface displacement data? A case study. Applied Computing and Geosciences **26**, 100242 (2025) https://doi.org/10.1016/j.acags.2025.100242

Singh, A.: Groundwater resources management through the applications of simulation modeling: A review. Science of The Total Environment **499**, 414–423 (2014) https://doi.org/10.1016/j.scitotenv.2014.05.048

Shivanand, S.K., Rosić, B., Matthies, H.G.: Stochastic modelling of symmetric positive definite material tensors. Journal of Computational Physics **505**, 112883 (2024) https://doi.org/10.1016/j.jcp.2024.112883

Tange, O.: GNU Parallel 20241122 ('Ahoo Daryaei'). https://doi.org/10.5281/zenodo.14207479 . GNU Parallel is a general parallelizer to run multiple serial command line programs in parallel without changing them. https://doi.org/10.5281/zenodo.14207479

Tarantola, A.: Inverse Problem Theory and Methods for Model Parameter Estimation. Other Titles in Applied Mathematics. Society for Industrial and Applied Mathematics, Philadelphia, PA (2005). https://doi.org/10.1137/1.9780898717921

Taghia, J., Ma, Z., Leijon, A.: Bayesian estimation of the von-mises fisher mixture model with variational inference. IEEE Transactions on Pattern Analysis and Machine Intelligence **36**(9), 1701–1715 (2014) https://doi.org/10.1109/TPAMI.2014.2306426

Tomás, R., Romero, R., Mulas, J., Marturià, J.J., Mallorquí, J.J., Lopez-Sanchez, J.M., Herrera, G., Gutiérrez, F., González, P.J., Fernández, J., Duque, S., Concha-Dimas, A., Cocksley, G., Castañeda, C., Carrasco, D., Blanco, P.: Radar interferometry techniques for the study of ground subsidence phenomena: a review of practical

issues through cases in Spain. Environmental Earth Sciences **71**(1), 163–181 (2014) https://doi.org/10.1007/s12665-013-2422-z

Varrette, S., Cartiaux, H., Peter, S., Kieffer, E., Valette, T., Olloh, A.: Management of an Academic HPC & Research Computing Facility: The ULHPC Experience 2.0. In: Proceedings of the 2022 6th High Performance Computing and Cluster Technologies Conference. HPCCT '22, pp. 14–24. Association for Computing Machinery, New York, NY, USA (2022). https://doi.org/10.1145/3560442.3560445

Linde, A.: DIC in variable selection. Statistica Neerlandica **59**(1), 45–56 (2005) https://doi.org/10.1111/j.1467-9574.2005.00278.x

Vehtari, A., Gelman, A., Gabry, J.: Practical bayesian model evaluation using leave-one-out cross-validation and WAIC. Statistics and computing **27**, 1413–1432 (2017) https://doi.org/10.1007/s11222-016-9696-4

Vehtari, A., Simpson, D., Gelman, A., Yao, Y., Gabry, J.: Pareto smoothed importance sampling. arXiv preprint arXiv:1507.02646 (2015). arXiv preprint arXiv:1507.02646

Watanabe, S.: WAIC and WBIC for mixture models. Behaviormetrika **48**(1), 5–21 (2021) https://doi.org/10.1007/s41237-021-00133-z

Watanabe, S., Opper, M.: Asymptotic equivalence of bayes cross validation and widely applicable information criterion in singular learning theory. Journal of machine learning research **11**(12) (2010)

Walker, G., Wang, Q.J., Horne, A.C., Evans, R., Richardson, S.: Estimating groundwater-river connectivity factor for quantifying changes in irrigation return flows in the Murray–Darling Basin. Australasian Journal of Water Resources **24**(2), 121–138 (2020) https://doi.org/10.1080/13241583.2020.1787702

Zhang, J., Yang, Y., Ding, J.: Information criteria for model selection. Wiley Interdisciplinary Reviews: Computational Statistics **15**(5), 1607 (2023) https://doi.org/10.1002/wics.1607